Proposed Rabi-Kondo Correlated State in a Laser-Driven Semiconductor Quantum Dot

B. Sbierski,[1,2] M. Hanl,[3] A. Weichselbaum,[3] H. E. Türeci,[1,4] M. Goldstein,[5] L. I. Glazman,[5] J. von Delft,[3] and A. İmamoğlu[1]

[1]*Institute for Quantum Electronics, ETH Zürich, CH-8093 Zürich, Switzerland*
[2]*Dahlem Center for Complex Quantum Systems and Institut für Theoretische Physik, FU Berlin, D-14195 Berlin, Germany*
[3]*Arnold Sommerfeld Center for Theoretical Physics and Center for NanoScience, LMU München, D-80333 München, Germany*
[4]*Department of Electrical Engineering, Princeton University, Princeton, New Jersey 08544, USA*
[5]*Department of Physics, Yale University, 217 Prospect Street, New Haven, Connecticut 06520, USA*

(Received 28 November 2012; published 10 October 2013)

Spin exchange between a single-electron charged quantum dot and itinerant electrons leads to an emergence of Kondo correlations. When the quantum dot is driven resonantly by weak laser light, the resulting emission spectrum allows for a direct probe of these correlations. In the opposite limit of vanishing exchange interaction and strong laser drive, the quantum dot exhibits coherent oscillations between the single-spin and optically excited states. Here, we show that the interplay between strong exchange and nonperturbative laser coupling leads to the formation of a new nonequilibrium quantum-correlated state, characterized by the emergence of a laser-induced secondary spin screening cloud, and examine the implications for the emission spectrum.

DOI: 10.1103/PhysRevLett.111.157402 PACS numbers: 78.60.Lc, 72.10.Fk, 78.40.Fy, 78.67.Hc

Introduction.—Exchange interactions between a singly occupied quantum dot (QD) and a fermionic bath (FB) of itinerant electrons in the bulk lead to the formation of a Kondo state $|K\rangle$ [1–3]. When this many-body ground state is coupled by a laser field of vanishingly small Rabi frequency Ω to an optically excited trion state $|T\rangle$ with an additional QD electron-hole pair [see Fig. 1(a)], the resulting emission spectrum at low FB temperatures T is highly asymmetric [4,5]. Within the energy range defined by Kondo temperature $T_K \gg T$, the spectral line shape is characterized by a power-law singularity. Anderson orthogonality (AO) determines the corresponding noninteger exponent and precludes any coherent light scattering in this limit. In the opposite limit of large Ω and vanishing exchange interaction ($T_K \to 0$), the emission spectrum consists of a Mollow triplet and an additional δ-function peak [6–8]. While the latter stems from coherent Rayleigh scattering, the Mollow triplet originates from incoherent transitions between dressed states which are superpositions of the original excited trion and the singly charged ground states.

In this Letter, we analyze the interplay between strong exchange and nonperturbative laser couplings. By using a combination of numerical and analytical techniques, we find that the emission line shape for $T \ll \Omega \ll T_K$ differs drastically from both the above limits. We demonstrate the emergence of a new quantum-correlated many-body state, which is a laser-induced, coherent superposition of the Kondo singlet state $|K\rangle$ and the trionic state $|T\rangle$ [see Fig. 1(a)]. The Kondo state involves a spin 1/2 on the dot, screened by a spin cloud in the FB which is formed within distance $\propto 1/T_K$ from the dot, while the FB is trivial in the bare trion state. The new quantum-correlated state is

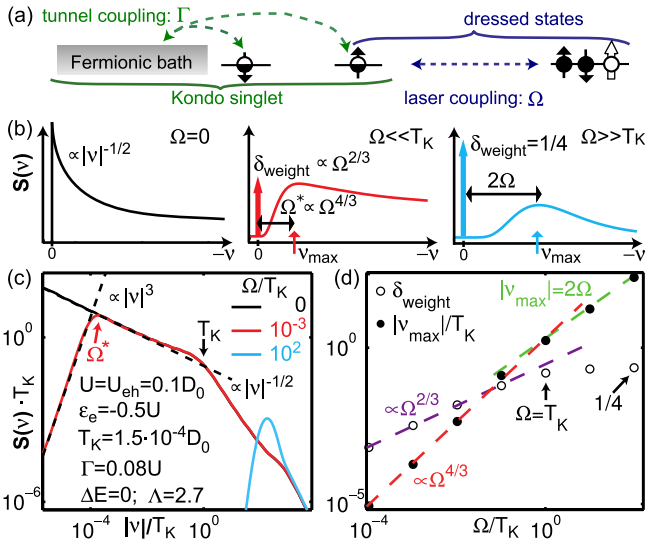

FIG. 1 (color online). (a) Competition between tunnel and laser coupling on the QD. While tunnel coupling favors a Kondo singlet state correlated with the FB, laser coupling favors dressed QD states. The characteristic energy scales are the Kondo temperature T_K and Rabi frequency Ω, respectively. (b) Schematic plots of emission spectra $S(\nu)$ from the Rabi-Kondo model Eq. (1) for $\Delta E = 0$ and three characteristic choices for Ω/T_K. For $\Omega = 0$, $S(\nu)$ shows a power-law divergence (left-hand panel). With increasing laser intensity ($\Omega \neq 0$, other two panels) it transforms to a δ peak at $\nu = 0$ (thick arrows) and a broad maximum at the (renormalized) Rabi frequency. (c),(d) NRG results with power-law asymptotes denoted as dashed lines: Log-log plot of the broad emission peak [$S(\nu < 0)$] (c), its position $|\nu_{\max}|$ (dots) and the δ-peak weight (circles) vs Ω/T_K (d). We have confirmed similar results for the nonsymmetric case $\varepsilon_e \neq -U/2$ and $U \neq U_{e\text{-}h}$ as long as $n_{e\uparrow} + n_{e\downarrow} - n_h \simeq 1$.

associated with the formation of an additional "secondary" screening cloud at larger distances that compensates for the differences in local occupancies between $|K\rangle$ and $|T\rangle$. The secondary screening process is also of the Kondo type, and sets in below a secondary Kondo temperature, the renormalized Rabi frequency $\Omega^* \propto \Omega^{4/3}$. This new energy scale manifests itself in the location of a broad peak in the emission spectrum. The peak's red and blue tails follow power-law functions corresponding to the primary and secondary Kondo correlations, respectively. The emergence of the secondary screening cloud coincides with the recovery of the δ-function peak in the emission spectrum, with weight scaling as $\Omega^{2/3}$. Measuring these effects should be possible in a setting similar to the one recently employed in Ref. [5]. There the effects of Kondo correlations on the absorption spectrum of self-assembled QDs were measured in the limit $\Omega < T$, and the ability to resolve spectral features at $T < T_K$ was demonstrated. Starting from this system one would need to increase the laser power to reach $\Omega > T$ while measuring the resulting resonance fluorescence spectrum, or, alternatively, employ a continuous-wave laser pump-probe setup.

Model.—We consider a self-assembled QD in a semiconductor heterostructure, tunnel coupled to a FB. We assume laser light propagating along the heterostructure growth direction with right-handed circular polarization $\sigma_L = +1$ and a frequency ω_L close to the QD trion (X^-) resonance. We model the system by an excitonic Anderson model [4,9] augmented by a nonperturbative laser-QD interaction in the rotating wave approximation. We set $\hbar = k_B = 1$ and assume zero magnetic field. Optical selection rules imply that only the spin-down valence electron state will be optically excited, leading to the generation of a trion state involving a spin-up hole [Fig. 1(a)]. The spontaneous emission rate γ_{SE} is assumed to be negligibly small compared to all other energy scales. In the rotating frame, the Hamiltonian, to be called the "Rabi-Kondo model," thus reads

$$H = \sum_{\sigma}(\varepsilon_e - U_{e\text{-}h}\hat{n}_h)\hat{n}_{e\sigma} + U\hat{n}_{e\uparrow}\hat{n}_{e\downarrow} + (\varepsilon_h - \omega_L)\hat{n}_h + \sum_{k\sigma}\varepsilon_{k\sigma}c^\dagger_{k\sigma}c_{k\sigma} + \sqrt{\Gamma/(\pi\rho)}\sum_{k\sigma}(e^\dagger_\sigma c_{k\sigma} + \mathrm{H.c.}) + \Omega e^\dagger_\downarrow h^\dagger_\Uparrow + \mathrm{H.c.} \quad (1)$$

The first line defines the QD Hamiltonian, where $\hat{n}_{e\sigma} = e^\dagger_\sigma e_\sigma$, $\hat{n}_h = h^\dagger_\Uparrow h_\Uparrow$, while $e^\dagger_\sigma$ and $h^\dagger_\Uparrow$ are, respectively, creation operators for QD spin-σ electrons ($\sigma = \uparrow, \downarrow$ or ± 1) and spin-up holes, ε_e and ε_h being the corresponding energies. We account for intradot Coulomb interaction by $U_{e\text{-}h} > 0$ and $U > 0$. To ensure a separated low-energy subspace formed by the states in Fig. 1(a), the laser detuning from the bare QD transition, $\delta_L = \omega_L - \varepsilon_e - U - \varepsilon_h + 2U_{e\text{-}h}$, has to be small in the sense defined below. The second line of Eq. (1) models a noninteracting conduction band (the FB) of energies $\varepsilon_{k\sigma} \in [-D_0, D_0]$, with $\varepsilon_F = 0$ and constant density of states $\rho \equiv 1/(2D_0)$ per spin, tunnel coupled to the QD's e level, giving it a width Γ. We assume $T \ll \Gamma \ll U \simeq U_{e\text{-}h} \ll D_0 \ll \varepsilon_h, \omega_L$ and investigate a situation where the QD carries one negative charge on average, $n_{e\uparrow} + n_{e\downarrow} - n_h \simeq 1$ [10]. The QD-laser coupling of strength Ω [last term of Eq. (1)] connects the trion and Kondo subspaces, with projectors $P_T = \hat{n}_h$ or $P_K = 1 - \hat{n}_h$. When $\Omega = 0$, these subspaces have hole and e-level occupancies $n^T_h = 1$ and $n^T_{e\sigma} \simeq 1$ or $n^K_h = 0$ and $n^K_{e\sigma} \simeq 1/2$, respectively, and ground states $|T\rangle$ and $|K\rangle$ with energy difference $\Delta E = E_{0,T} - E_{0,K}$.

Emission spectrum.—The emission spectrum at detuning ν from the laser frequency ω_L is proportional to the spectral function

$$S(\nu) = \sum_{n,m}\varrho_m |\langle n|h_\Uparrow e_\downarrow|m\rangle|^2 \delta(E_n - E_m + \nu), \quad (2)$$

where $|m\rangle$ and E_m are eigenstates and eigenenergies of the Rabi-Kondo model. We assume that spontaneous emission has a negligible effect on the system's steady state, which is taken to be a thermal state in the rotating frame at the temperature T of the solid state environment, $\varrho_m = Z^{-1}e^{-E_m/T}$ [9], and concentrate on $T = 0$. To simplify the discussion we will address mostly the $\Delta E = 0$ case below (achieved by properly tuning the laser frequency ω_L to resonance), where the secondary screening effect is most pronounced, and defer the treatment of finite ΔE to the Supplemental Material [9]. Figure 1(b) schematically summarizes the main features of typical numerical renormalization group (NRG) [11–13] results for the emission spectrum in Figs. 1(c) and 1(d).

For $\Omega \gg T_K$, no signatures of Kondo physics are expected. The emission spectrum can be completely understood in terms of a dressed state ladder with the assumption $\gamma_{\mathrm{SE}} = 0$ and an intramanifold, FB-induced decay process [14,15]. The spectrum has two peaks: a broad peak at $|\nu_{\max}| = 2\Omega$ and a δ peak at $\nu = 0$, both with equal weight 0.25 [see Fig. 1(b), blue line].

The situation is much more interesting for the Kondo-dominated regime, $\Omega \ll T_K$, which we consider henceforth. Here one might attempt to treat the QD-laser coupling [last term in Eq. (1)] as a perturbation. This would yield a spectrum that is essentially the same as the $\Omega = 0$ spectrum calculated in Ref. [4]. However, we will show momentarily that this is correct only if the frequency $|\nu|$ is larger than a new energy scale $\Omega^* \ll T_K$.

Effective model.—In order to understand this restriction on the perturbative treatment of the QD-laser coupling, as well as to derive the low-frequency behavior, we introduce an effective Hamiltonian H', which captures the essential physics of H in the entire regime $|\nu| < T_K$. It can be thought of as the result of integrating out the degrees of freedom in the Rabi-Kondo model H with energies larger

than T_K. We can concentrate on just two states of the QD together with the surrounding FB degrees of freedom: the Kondo singlet state restricted (subscript r) to a FB region of screening cloud size $\lesssim 1/T_K$, $|K\rangle_r$, and the trion state $|T\rangle_r$, with no screening cloud. We thus replace the QD and the nearby degrees of freedom of the FB by a two level system (TLS) whose $\sigma'_z = \pm 1$ (σ'_i being the Pauli matrices) eigenstates correspond to the $|T\rangle_r$ and $|K\rangle_r$, respectively. These are coupled by the laser and are split in energy. Furthermore, the outer electrons with energies $\lesssim T_K$ experience different scattering phase shifts depending on the state of the TLS. Taking $|K\rangle_r$ as reference state relative to which phase shifts are measured, we have $\delta^K_\sigma = 0$ and, by the Friedel sum rule [16], $\delta^T_\sigma = \Delta_\sigma \pi$, where $\Delta_\sigma = (n^T_{e\sigma} - \delta_{\sigma\downarrow}) - n^K_{e\sigma} = \sigma/2$ is the total dot charge difference per spin between $|T\rangle_r$ and $|K\rangle_r$. All this is captured by the following Hamiltonian:

$$H' = \sum_{k\sigma} \varepsilon'_{k\sigma} c'^{\dagger}_{k\sigma} c'_{k\sigma} + \Omega' \sigma'_x + \frac{\Delta E'}{2} \sigma'_z + P'_T \sum_{\sigma,k,k'} U'_\sigma c'^{\dagger}_{k\sigma} c'_{k'\sigma}. \tag{3}$$

The first term describes the FB degrees of freedom whose distance from the QD is larger than $\sim 1/T_K$, corresponding to a reduced half-bandwidth $D'_0 \sim T_K$. The second term describes optical excitations, with $\Omega' = \Omega_r \langle K|h_{\Uparrow} e_{\downarrow}|T\rangle_r \propto \Omega$. The third term is the detuning, $\Delta E' = \Delta E$ [17]. Finally, the last term accounts for the scattering of the FB electrons by the TLS, where $P'_T = (1 + \sigma'_z)/2$ is a projector onto the trion sector. To reproduce the phase shifts mentioned above, we choose U'_σ equal to $-\sigma$ times a large positive numerical value ($\gg D'_0$) which satisfies $\pi \rho' U'_\sigma = -\tan(\Delta_\sigma \pi)$. NRG energy flow diagrams confirm that H' is a good description of the system below T_K [9]. For $|\nu| < T_K$, the emission spectrum $S(\nu)$ for the Rabi-Kondo model is reproduced qualitatively by $S'(\nu)$ computed as in Eq. (2), with H' and σ'_- replacing H and $h_{\Uparrow} e_{\downarrow}$, respectively, [9].

Intermediate-frequency behavior and emergence of a new energy scale.—To lowest order in Ω', the behavior of $S'(\nu)$ is governed by the AO between the TLS states $|K\rangle_r$ and $|T\rangle_r$, caused by the difference in phase shifts the FB electrons experience in the two states. The spectrum thus behaves as a power law, $S'(\nu) \sim |\nu|^{2\eta'_x - 1}$, with AO exponent $2\eta'_x = [\delta^K_\uparrow - \delta^T_\uparrow]^2/\pi^2 + [\delta^K_\downarrow - \delta^T_\downarrow]^2/\pi^2 = 1/2$ [13,18], in agreement with the $\Omega = 0$ results of Ref. [4]. This implies that the hybridization operator σ'_x has a scaling dimension $\eta'_x = 1/4 < 1$ and is thus a relevant perturbation near the fixed point $\Omega' = 0$. Thus the leading-order renormalization group flow equation for Ω' as one decreases the cutoff D' from its bare value D'_0 is [19]

$$D' \frac{d}{dD'} \left(\frac{\Omega'}{D'} \right) = (\eta'_x - 1) \frac{\Omega'}{D'}. \tag{4}$$

The dimensionless coupling Ω'/D' therefore grows and becomes of order 1 when the cutoff reaches the scale

$$\Omega^* = D'_0 \left(\frac{\Omega'}{D'_0} \right)^{1/(1-\eta'_x)} \sim T_K \left(\frac{\Omega}{T_K} \right)^{4/3} \ll T_K. \tag{5}$$

Hence, one may treat the term $\Omega' \sigma'_x$ [corresponding to the last term in Eq. (1)] as a perturbation only if $|\nu| \gg \Omega^*$. The power law $S(\nu) \sim |\nu|^{-1/2}$ thus applies at intermediate frequencies, $\Omega^* \ll |\nu| \ll T_K$. The power-law divergence of the spectrum is cut off around $|\nu| \sim \Omega^*$ [13], resulting in a maximum in the spectrum at this scale, as confirmed by the NRG data shown in Fig. 1. The emergence of this new energy scale is one of our central results. At low frequencies, $|\nu| \ll \Omega^*$, the physics is governed by a new fixed point, which we now discuss.

Secondary Kondo screening.—To understand this new fixed point we formally argue below that H' can be mapped onto the anisotropic Kondo model. This "secondary" Kondo model should not be confused with the original "primary" isotropic Kondo model for the QD spin. The role of the secondary Kondo temperature is played by Ω^*; at energies below Ω^*, the original system flows to a strong-coupling fixed point featuring strong hybridization of Kondo and trion sectors, as confirmed by NRG level-flow data [9]. The low-energy behavior is universal when energies are measured in units of Ω^*.

One of the predictions of this secondary Kondo picture is that the ground state of H for $\Omega \ll T_K$ and $\Delta E = 0$ is an equal-amplitude superposition of the Kondo and trion states, with some secondary screening cloud, whose distance from the QD is larger than the primary Kondo length $\propto 1/T_K$. To understand this nested screening cloud structure, consider $|K\rangle$ (ground state for $\Omega = 0$, $\Delta E > 0$) as a reference state where the QD valence levels are filled and its conduction levels carry half an electron of each spin. Since the total spin is zero, the correlation function between the QD spin and the total FB spin is $\langle S^z_{\rm QD} S^z_{\rm FB} \rangle = \langle S^z_{\rm QD} (S^z_{\rm FB} + S^z_{\rm QD}) \rangle - \langle (S^z_{\rm QD})^2 \rangle = -\langle (S^z_{\rm QD})^2 \rangle = -1/4$. This implies that when projecting into the subspace with spin-up (spin-down) in the QD, the FB has a net additional single spin-down (spin-up) electron [20] within a screening cloud up to a distance $\propto 1/T_K$ from the QD [indicated by ellipses in Fig. 2(a)]. If, on the other hand, $\Omega = 0$ but $\Delta E < 0$, the system is in the trion state $|T\rangle$ with two QD electrons and a spin-up hole, and no screening cloud [Fig. 2(b)]. The absorbed $\sigma_L = +1$ photon induces a change in QD charge per spin of Δ_σ, thus causing the phase shifts $\delta^T_\sigma = \sigma\pi/2$ with respect to the reference state, as mentioned above. Turning on the laser source Ω, when $\Delta E = 0$, the ground state is an equal-amplitudes superposition of the Kondo and trion states ($\langle P_T \rangle = \langle P_K \rangle = 1/2$), as depicted in Fig. 2(c). In analogy with the screening of a QD spin in a Kondo singlet, the FB screens the spin configurations of the $|T\rangle_r$ and $|K\rangle_r$ states, which, respectively, have spin $\sigma/4$ or $-\sigma/4$ with respect to their mutual average of $\sigma/4$, by

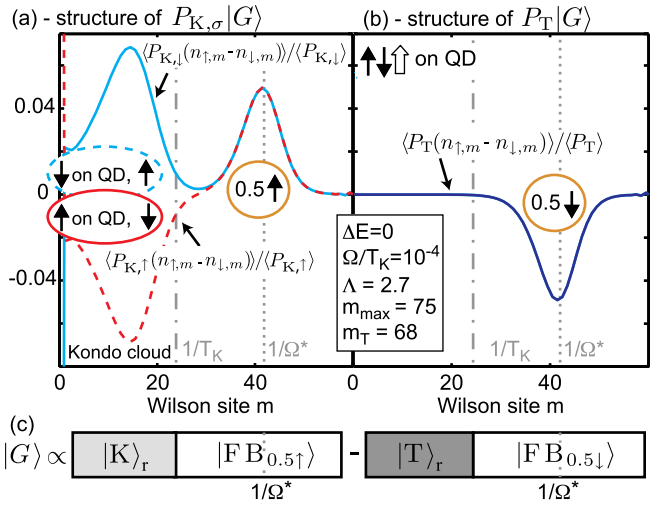

FIG. 2 (color online). NRG results for the Rabi-Kondo model Eq. (1). Distribution of magnetization $n_{\uparrow,m} - n_{\downarrow,m}$ along the Wilson chain, obtained after acting with QD projectors (a) $P_{K,\sigma} = P_K \hat{n}_{e,\sigma}(1 - \hat{n}_{e,\bar{\sigma}})$ and (b) P_T, for $\Omega/T_K = 10^{-4}$ and $\Delta E = 0$ at $T = 2 \times 10^{-14} D_0$ (corresponding to the energy scale of Wilson site $m_T = 68$). Even-odd oscillations have been averaged out. The QD is represented by site zero. In (a), the Kondo state, restricted to a region of size $\lesssim 1/T_K$ (subscript r), approximately $|K\rangle_r \propto |\uparrow\rangle|\mathrm{FB}_\downarrow\rangle_r - |\downarrow\rangle|\mathrm{FB}_\uparrow\rangle_r$, features a singlet configuration with FB magnetization opposite to that of the QD (left dip or peak structure). In (b) the $|T\rangle_r$ trivial FB configuration appears within the same length scale. The presence of a laser ($\Omega > 0$) combines the states $|K\rangle_r$ and $|T\rangle_r$ into a new ground state shown in (c), where FB states $|\mathrm{FB}_{0.5\sigma}\rangle$ carry a magnetization of *half* a spin σ at distance $1/\Omega^*$ [peak in (a), dip in (b)]. The spin orientation of this secondary screening cloud is controlled by the laser polarization $\sigma_L = +1$.

creating FB spin configurations with an opposite spin of $-\sigma/4$ or $\sigma/4$ (i.e., *half* an electron spin) within distance $\sim 1/\Omega^*$ of the QD, respectively, [21]. This nested screening cloud indeed appears in the NRG results in Fig. 2, further confirming our effective low-energy description.

Low-frequency behavior and δ peak.—To derive the low-frequency behavior of the spectrum, as well as the appearance of the elastic δ peak mentioned in the introduction, we make the notion of "secondary Kondo effect" more precise. This can be done formally by transforming H' into a secondary Kondo model in two stages: (i) Upon bosonization of the FB [22] H' becomes the spin-boson model with Ohmic dissipation [23,24], the basic idea behind this mapping being that the low-lying particle-hole excitations of the FB are bosonic in nature, with a linear (Ohmic) density of states, and (ii) the spin-boson model can be mapped onto the anisotropic Kondo model [1,2]:

$$H'_K = -i v_F \sum_{\sigma=\uparrow,\downarrow} \int dx \psi^\dagger_\sigma(x) \partial_x \psi_\sigma(x) + \frac{J_z}{2} S'_z s'_z(0) + \frac{J_{xy}}{2} S'_- s'_+(0) + \mathrm{H.c.} - \Delta E_z S'_z, \quad (6)$$

where $v_F = 1/(\pi\rho')$ is the Fermi velocity, S'_i are the components of the secondary Kondo impurity spin, and $s'_i(0) = \sum_{\sigma,\sigma'} \psi_\sigma(0)^\dagger \tau_i^{\sigma\sigma'} \psi_{\sigma'}(0)/2$ (τ_i being the Pauli matrices) are the FB spin density components in the vicinity of the impurity. Under this mapping $\sigma'_z = 2S'_z$ (hence, $\Delta E_z \propto \Delta E'$), but $\sigma'_+ \to S'_+ s'_-(0)$.

One can now use known results on H'_K to find the low-frequency ($|\nu| \ll \Omega^*$) behavior of the emission spectrum of H'. By the above mapping $S'(\nu)$ is proportional to the spectral function of the retarded correlator of $S'_+ s'_-(0)$ with its conjugate in H'_K. Since the anisotropic antiferromagnetic Kondo problem flows to the same strong-coupling fixed point as the isotropic version, the calculation of low-frequency power-law exponents can be done in the isotropic case $J_z = J_{xy}$, where the $S'_+ s'_-(0)$ correlator can be replaced by the $S'_z s'_z(0)$ correlator. At low energies, after the impurity spin is screened by the FB, $S'_z s'_z(0)$ can be replaced by the square of the local density of the z component of the electronic spin, which is a four-fermion operator. Thus, if the effective magnetic field vanishes, $\Delta E_z = 0$, its correlation function scales at long times ($t > 1/\Omega^*$) as t^{-4}, leading to a $\sim|\nu|^3$ low-frequency behavior of the corresponding spectral function. The same then applies to $S^{(\prime)}(\nu)$ in the regime $|\nu| \ll \Omega^*$. This is indeed the behavior of the NRG results, cf. Fig. 1(c) and Ref. [9].

The above picture leads to another implication for the spectrum: Since the relevant perturbation $\Omega' \sigma'_x$ strongly hybridizes, and thus cuts off the AO between the $|K\rangle$ and $|T\rangle$ states at energy scales smaller than Ω^* [13], a Dirac δ peak is now allowed to appear in the spectrum at $\nu = 0$. By the definition of $S'(\nu)$, its weight is $\delta_{\mathrm{weight}} = |\langle\sigma'_x\rangle|^2$. Since Ω^* is the only low-energy scale, we expect that $\Omega' \langle\sigma'_x\rangle \propto \Omega^* \propto \Omega'^{4/3}$. Hence, $\langle\sigma'_x\rangle \propto \Omega'^{1/3} \propto \Omega^{1/3}$, leading to $\delta_{\mathrm{weight}} \propto \Omega^{2/3}$, which is in excellent agreement with the NRG results, Fig. 1(d) [25,26].

Conclusions.—Laser excitation of a QD in the Kondo regime leads to a new correlated state featuring a nested spin screening cloud in the FB (Fig. 2) and gives rise to a specific double-peaked emission line shape (Fig. 1): (i) a broad peak centered at a renormalized Rabi frequency Ω^* [Eq. (5)], with a $\sim|\nu|^{-1/2}$ red tail, resulting from the AO between ground and postemission states resembling $|T\rangle$ and $|K\rangle$ at length scales $\ll 1/\Omega^*$. A Fermi-liquid-type blue tail stems from the cutoff of the AO by the relevant Rabi coupling, as ground and postemission states share a "common" FB configuration at length scales $\gg 1/\Omega^*$ due to the secondary screening cloud. (ii) This common FB region leads to a δ peak at $\nu = 0$ with weight $\propto \Omega^{2/3}$. The Ω dependence of the coherent Rayleigh scattering strength in the presence of a finite spontaneous emission rate γ_{SE} remains an open question.

We acknowledge helpful discussions with A. Rosch. This work was supported by an ERC Advanced

Investigator Grant (B. S. and A. I.). H. E. T. acknowledges support from the Swiss NSF under Grant No. PP00P2-123519/1. M. G. is supported by the Simons Foundation and the BIKURA (FIRST) program of the Israel Science Foundation, L. I. G. by NSF DMR Grants No. 0906498 and No. 1206612, and J. v. D., M. H., and A. W. by the DFG via NIM, SFB631, SFB-TR12, and WE4819/1-1.

[1] A. Hewson, *The Kondo Problem to Heavy Fermions* (Cambridge University Press, Cambridge, England, 1993).
[2] D. L. Cox and A. Zawadovski, Adv. Phys. **47**, 599 (1998).
[3] L. Kouwenhoven and L. Glazman, Phys. World **14**, 33 (2001).
[4] H. E. Türeci, M. Hanl, M. Claassen, A. Weichselbaum, T. Hecht, B. Braunecker, A. Govorov, L. Glazman, A. Imamoglu, and J. von Delft, Phys. Rev. Lett. **106**, 107402 (2011).
[5] C. Latta *et al.*, Nature (London) **474**, 627 (2011).
[6] B. R. Mollow, Phys. Rev. **188**, 1969 (1969).
[7] E. B. Flagg, A. Muller, J. W. Robertson, S. Founta, D. G. Deppe, M. Xiao, W. Ma, G. J. Salamo, and C. K. Shih, Nat. Phys. **5**, 203 (2009).
[8] C. Matthiesen, A. N. Vamivakas, and M. Atatüre, Phys. Rev. Lett. **108**, 093602 (2012).
[9] See Supplemental Material at http://link.aps.org/supplemental/10.1103/PhysRevLett.111.157402 for additional discussion of the Rabi-Kondo model H, the case of finite ΔE, the effective model H' with its emission spectrum, NRG flow diagrams and the theory of quantum quenches.
[10] This requires $\Gamma \ll -\varepsilon_e,\ \varepsilon_e + U,\ -(2\varepsilon_e - 2U_{e\text{-}h} + U),\ -\varepsilon_e + U_{e\text{-}h} - U$.
[11] R. Bulla, T. A. Costi, and T. Pruschke, Rev. Mod. Phys. **80**, 395 (2008).
[12] A. Weichselbaum and J. von Delft, Phys. Rev. Lett. **99**, 076402 (2007); A. Weichselbaum, Phys. Rev. B **86**, 245124 (2012).
[13] W. Münder, A. Weichselbaum, M. Goldstein, Y. Gefen, and J. von Delft, Phys. Rev. B **85**, 235104 (2012).
[14] B. Sbierski and A. Imamoglu (to be published).
[15] In the more realistic situation of a finite rate γ_{SE}, a Mollow *trip*let with a broadened peak at $\nu = 0$ and a blue detuned peak at $\nu = 2\Omega$ may develop.
[16] J. Friedel, Philos. Mag. **43**, 153 (1952); Can. J. Phys. **34**, 1190 (1956); D. C. Langreth, Phys. Rev. **150**, 516 (1966).
[17] More precisely, an offset is added to $\Delta E'$ such that $H'|_{\Omega',\Delta E'=0}$ has a ground state degenerate in the two TLS sectors.
[18] B. Roulet, J. Gavoret, and P. Nozières, Phys. Rev. **178**, 1072 (1969); P. Nozières, J. Gavoret, and B. Roulet, *ibid.* **178**, 1084 (1969); P. Nozières and C. T. De Dominicis, *ibid.* **178**, 1097 (1969).
[19] J. Cardy, *Scaling and Renormalization in Statistical Physics* (Cambridge University Press, Cambridge, England, 1996).
[20] I. Affleck, arXiv:0911.2209.
[21] The total electron number is of course integer; if the screening cloud contains fractions of electrons, the rest is spread over the entire system, and thus does not contribute to the charge and spin distributions in the thermodynamic limit.
[22] A. Gogolin, A. A. Nersesyan, and A. M. Tsvelik, *Bosonization and Strongly Correlated Systems* (Cambridge University Press, Cambridge, England, 1998).
[23] U. Weiss, *Quantum Dissipative Systems* (World Scientific, Singapore, 1999).
[24] A. Leggett, S. Chakravarty, A. Dorsey, M. Fisher, A. Garg, and W. Zwerger, Rev. Mod. Phys. **59**, 1 (1987).
[25] The Ω scaling of the δ-peak weight can also be found as follows: it scales as the spectral weight that goes missing from the $\Omega = 0$ emission spectrum $\propto |\nu|^{-1/2}$ when the latter is cut off at $\nu \simeq \Omega^*$: $\int_0^{\Omega^{4/3}} d\nu \nu^{-1/2} \propto \Omega^{2/3}$.
[26] However, further work including spontaneous emission in the theoretical treatment would have to revisit the actual form of the spectrum for $|\nu| < \gamma_{\mathrm{SE}}$ and the distribution of δ_{weight} into an elastic and inelastic contribution.

Supplemental Material: "Proposed Rabi-Kondo Correlated State in a Laser-Driven Semiconductor Quantum Dot"

Discussion of the Hamiltonian H and Born-Markov approximation

Here we discuss the form of the Rabi-Kondo model Hamiltonian H, Eq. (1) in the main text, in more detail. The QD part reads $H_{\rm QD} = \sum_\sigma \left(\varepsilon_{\rm e} - U_{\rm eh} n_{\rm h}\right) n_{{\rm e}\sigma} + U n_{{\rm e}\uparrow} n_{{\rm e}\downarrow} + \varepsilon_{\rm h} n_{\rm h}$. The eigenenergies are conveniently displayed vs. the gate voltage which controls $\varepsilon_{\rm e}$ and $\varepsilon_{\rm h}$, in Fig. S1(a). The lowest energy QD state in the subspace with hole number $n_{\rm h} = 0$ or 1 is denoted by a purple or blue solid line, respectively. We focus on a gate voltage regime around V_0, as marked in Fig. S1(a). In this regime the lowest energy QD states carry one negative charge. Applying a monochromatic laser with photon energy $\omega_{\rm L} \simeq \varepsilon_{\rm h}$ leads to the rotating frame Hamiltonian $H_{\rm QD,L} = \sum_\sigma \left(\varepsilon_{\rm e} - U_{\rm eh} n_{\rm h}\right) n_{{\rm e}\sigma} + U n_{{\rm e}\uparrow} n_{{\rm e}\downarrow} + \left(\varepsilon_{\rm h} - \omega_{\rm L}\right) n_{\rm h}$, effectively shifting the purple line to the vicinity of the blue line. If the detuning $\delta_{\rm L}$ to the bare QD transition is small, then there exists a low energy description of $H_{\rm QD,L}$ involving only the states $|\uparrow\rangle, |\downarrow\rangle$ and the trion $|\uparrow\downarrow\Uparrow\rangle$ shown in Fig. 1(a) of the main text.

We now add to $H_{\rm QD,L}$ the QD-laser coupling in rotating wave approximation, $H_{\rm QD-L} = \Omega e_\downarrow^\dagger h^\dagger + {\rm h.c.}$, (we assume a circularly polarized laser and apply optical selection rules to simplify the problem, see main text) and a radiative reservoir $H_{\rm rad}$ (leading to a spontaneous emission rate $\gamma_{\rm SE}$ on the order of $1\mu eV$). For $\Omega \gg \gamma_{\rm SE}$ a three-peak Mollow triplet, similar to the red curve in Fig. S1(b), can be detected in the RF spectrum. The central peak appears at the laser frequency, $\omega = \omega_{\rm L}$ and the two side peaks at detuning $\nu = \omega - \omega_{\rm L} = \pm 2\Omega$.

If we now include the fermionic bath (FB), $H_{\rm FB} = \sum_{k\sigma} \varepsilon_{k\sigma} c_{k\sigma}^\dagger c_{k\sigma}$, and the QD-FB hybridization $H_{\rm QD-FB}$, the Hamiltonian reads $H + H_{\rm rad}$ with H as in Eq. (1) of the main text. For a weak QD-FB coupling and temperatures $T > T_{\rm K}$ we make a Born-Markov approximation for the QD-FB coupling [1, 2], the corresponding transition rates in the dressed-QD Master equation crucially rely on the ratio between laser Rabi frequency Ω and sample temperature T. While $\Omega \ll T$ leads to a broadening of the ordinary Mollow RF-spectrum by symmetric thermal rates $\gamma_{\rm T}$ in each dressed-state manifold, a dominant laser $\Omega \gg T$ results in asymmetric intra-manifold rates γ_Ω and an asymmetric doublet in the RF spectrum, see Fig. S1(b), along with the dressed-state schematics. In this case, the FB cannot provide the energy difference for an upward transition between the dressed states. In experiment, the formation of an asymmetric doublet would have to be carefully distinguished from the effect of a finite laser detuning [which we have set to zero in Fig. S1(b)].

To access Kondo physics, $T < T_{\rm K}$ is required and the Born-Markov treatment of the dressed QD-FB interaction is no longer valid. With the spectral function defined as

$$S(\nu) = \frac{1}{2\pi} \int_{-\infty}^{\infty} d\tau \left\langle (h e_\downarrow)^\dagger(\tau) \, (h e_\downarrow) \right\rangle_{\rm ss} e^{-i\nu\tau}. \tag{S1}$$

the RF-spectrum is given by $\gamma_{\rm SE} \cdot S(\nu)$ [3]. Here, the occurrence of $\gamma_{\rm SE}$ shows that $H_{\rm rad}$ has explicitly been used in the derivation. If the coupling to the radiative reservoir is weak (i.e. $\gamma_{\rm SE}$ smaller than all other energy scales), we neglect $H_{\rm rad}$ to higher order in Eq. (S1), i.e. we approximate $(h e_\downarrow)^\dagger(\tau) \simeq e^{i\tau H} (h e_\downarrow)^\dagger e^{-i\tau H}$. Further, a similar approximation is done for the steady state density matrix $\rho_{\rm ss}$ used in

Eq. (S1) ($\langle ... \rangle_{\rm ss}$ denotes a trace over $\rho_{\rm ss}$): We assume that thermalization of the system due to the solid state environment at temperature T takes place on timescales much faster than spontaneous emission. Then, we neglect $H_{\rm rad}$ for $\rho_{\rm ss}$ and assert that

$$\rho_{\rm ss} = \rho_{\rm eq} = e^{-H/T} / {\rm Tr}\left(e^{-H/T}\right) \tag{S2}$$

serves as a good approximation of the steady state. This leads to a RF spectrum that has support for $\nu \lesssim T$ only. We will further discuss effects related to the neglect of $H_{\rm rad}$ in the last section of this Supplemental Material.

With these two important simplifications, the numerical study is facilitated considerably, Eq. (S1) can be written in Lehmann form and we arrive at Eq. (2) of the main text where the eigenstates and -energies of H (as computed approximately by NRG) are used.

To conclude, the main text investigates how the asymmetric two peak structure (blue line in Fig. S1(b) for $\Omega \gg T > T_{\rm K}$) changes when we increase the QD-FB coupling beyond perturbatively weak values, i.e. increase $T_{\rm K}$ above T. We investigate the more interesting regime $T_{\rm K} \gg \Omega$ in detail and comment briefly on the case $T_{\rm K} \ll \Omega$.

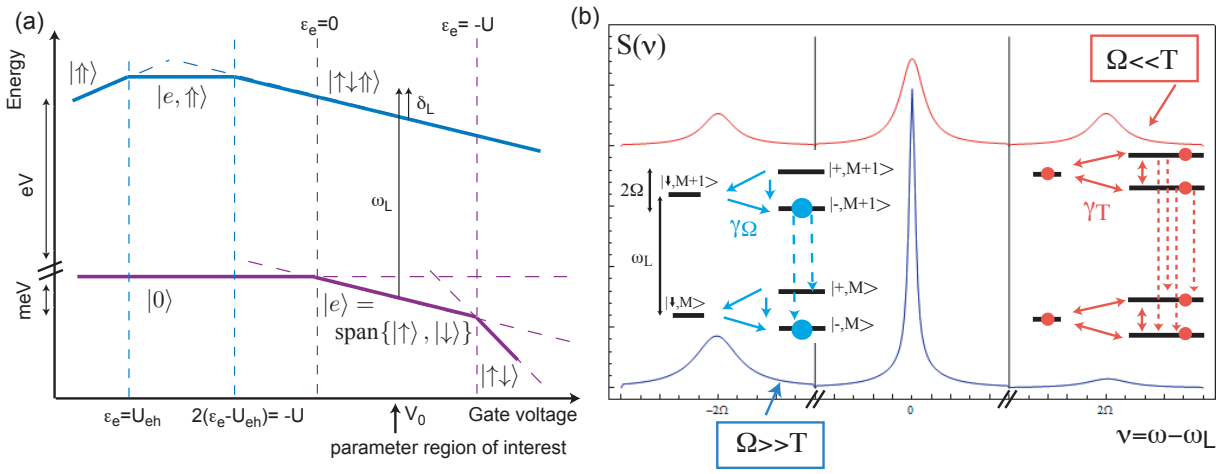

Figure S1: (a) Energy level diagram for $H_{\rm QD}$ vs. gate voltage. We assume that the gate voltage is tuned to the vicinity of V_0 where the ground state of $H_{\rm QD}|_{n_{\rm h}=0}$ and $H_{\rm QD}|_{n_{\rm h}=1}$ carries one negative charge, $\omega_{\rm L}$ is the laser frequency and $\delta_{\rm L}$ the detuning from the bare QD-transition. (b) Application of a resonant laser ($\delta_{\rm L} = 0$) and weak coupling to a FB at temperature $T \gg T_{\rm K}$ leads to formation of QD dressed states $|\pm\rangle = (|\uparrow\downarrow\Uparrow\rangle \pm |\uparrow\rangle)/\sqrt{2}$ where $|\uparrow\rangle$ and $|\downarrow\rangle$ denote QD states carrying one electron of spin up or down, respectively, while $|\uparrow\downarrow\Uparrow\rangle$ denotes a negatively charged exciton including a hole. The index M or $M-1$ counts the number of excitations (i.e. laser photons + holes), see [3], Ch. VI. Intra-manifold rates induced by the FB are denoted by solid arrows, steady state population by filled circles and spontaneous emission transitions by dashed arrows. The RF spectrum calculated using a Markovian master equation (neglecting Kondo correlations) shows a broadened Mollow triplet for $T_{\rm K} \ll \Omega \ll T$ (red) and an asymmetric doublet for $\Omega \gg T \gg T_{\rm K}$ (blue).

NRG energy flow diagrams for the Rabi-Kondo model H

The numerical renormalization group (NRG) is a method to approximately diagonalize quantum impurity Hamiltonians where a few-level system, described by $H_{\rm imp}$ (the impurity - or, in modern literature, the QD) is coupled to a (fermionic) bath, $H = H_{\rm imp} + H_{\rm imp-FB} + H_{\rm FB}$ [4]. The strategy is to approximate $H_{\rm FB}$ by

a tight-binding (Wilson-)chain where the coupling between two successive sites is exponentially decreasing as $\Lambda^{-n/2}$ for site index n, where $\Lambda > 1$ is a non-physical NRG discretization parameter. The QD is included as a site with index zero, only coupled to the first FB Wilson site (QD plus first FB Wilson site will be called "odd" Wilson chain). Each Wilson site can be identified with an exponentially decreasing energy scale $\Lambda^{-n/2}$, or, by looking at the associated fermionic wavefunction, with an exponentially increasing spatial separation $\Lambda^{n/2}$ from the QD position.

Due to the separation of energy scales along the Wilson chain, the chain Hamiltonian H_N, restricted to the first N sites, can be diagonalized iteratively. After multiplying H_N by $\Lambda^{N/2}$, the lowest eigenenergies can be plotted vs. N in an NRG energy flow diagram, thus showing high to low energy scales of H from left to right. Moreover, as a Wilson site can also be identified with a length scale in the impurity problem, the NRG flow accesses physics at increasing spatial separation from the impurity site with increasing N. Regions in which the rescaled eigenenergies form parallel horizontal lines are called fixed points - they can be described by fixed point Hamiltonians which are invariant under the renormalization group transformation.

Compared to computations of the quench spectral function in Ref. [5] for $\Omega = 0$, there are considerable conceptual changes for the computation in the $\Omega > 0$ case, described by the Rabi-Kondo model Hamiltonian, written as

$$H = \begin{pmatrix} H_{\mathrm{T}} & \Omega e_{\downarrow}^{\dagger} h_{\Uparrow}^{\dagger} \\ \Omega h_{\Uparrow} e_{\downarrow} & H_{\mathrm{K}} \end{pmatrix}. \tag{S3}$$

Most important is the loss of a quench setup between initial and final Hamiltonian, meaning that the hole is to be treated as a dynamic quantity. The NRG calculation in [5] relied on two separate NRG runs, separately diagonalizing the initial and final Hamiltonian given by $H_{\mathrm{K}} \equiv P_{\mathrm{K}} H P_{\mathrm{K}}$ and $H_{\mathrm{T}} \equiv P_T H P_T$, respectively. Then the corresponding two sets of eigenstates and -energies entered the analogue of Eq. (2). For $\Omega > 0$, however, we have to use only *one* NRG run for the full Hamiltonian H. Since this technical change comes with a number of important consequences, we first discuss these issues in the simple $\Omega = 0$ case.

For $\Omega = 0$, we define the ground state energy difference between H_{T} and H_{K} as

$$\Delta E \equiv E_{0,\mathrm{T}} - E_{0,\mathrm{K}} \tag{S4}$$

which has two contributions: On the one hand, the laser detuning δ_{L} from the bare QD transition affects ΔE trivially, on the other hand, a hybridization $\Gamma > 0$ causes Kondo correlations in the H_{K} Kondo singlet ground state $|\mathrm{K}\rangle$ that additionally lower its energy. The energy level diagram is shown in Fig. S2(a) for $\Delta E > 0$ (laser tuned to bare QD transition, $\delta_{\mathrm{L}} = 0$) and $\Delta E = 0$ (b). Note that with a single logarithmic discretization, only low-lying eigenstates close to the overall ground state energy are resolved with increasing accuracy (orange rungs in Fig. S2 are NRG energy eigenvalues). This means if we use for example $\delta_{\mathrm{L}} = 0$ ($\Delta E > 0$), as shown in (a), the state $|\mathrm{K}\rangle$ is well resolved while the $|\mathrm{T}\rangle$ state is not well described in NRG and does not have a reasonable steady state population since $\rho_{\mathrm{ss}} \propto e^{-H/T}$. Numerically feasible is the case shown in (b). Using a laser blue-detuned with respect to the bare QD transition ($\delta_{\mathrm{L}} > 0$), one can counteract the correlation energy and push the $|\mathrm{K}\rangle$ up (relative to $|\mathrm{T}\rangle$) to

adjust $\Delta E = 0$. This leads to good resolution and finite population for both ladders, as the steady state expectation values $\langle P_{\mathrm{K}} \rangle \simeq 0.5 \simeq \langle P_{\mathrm{T}} \rangle$ show.

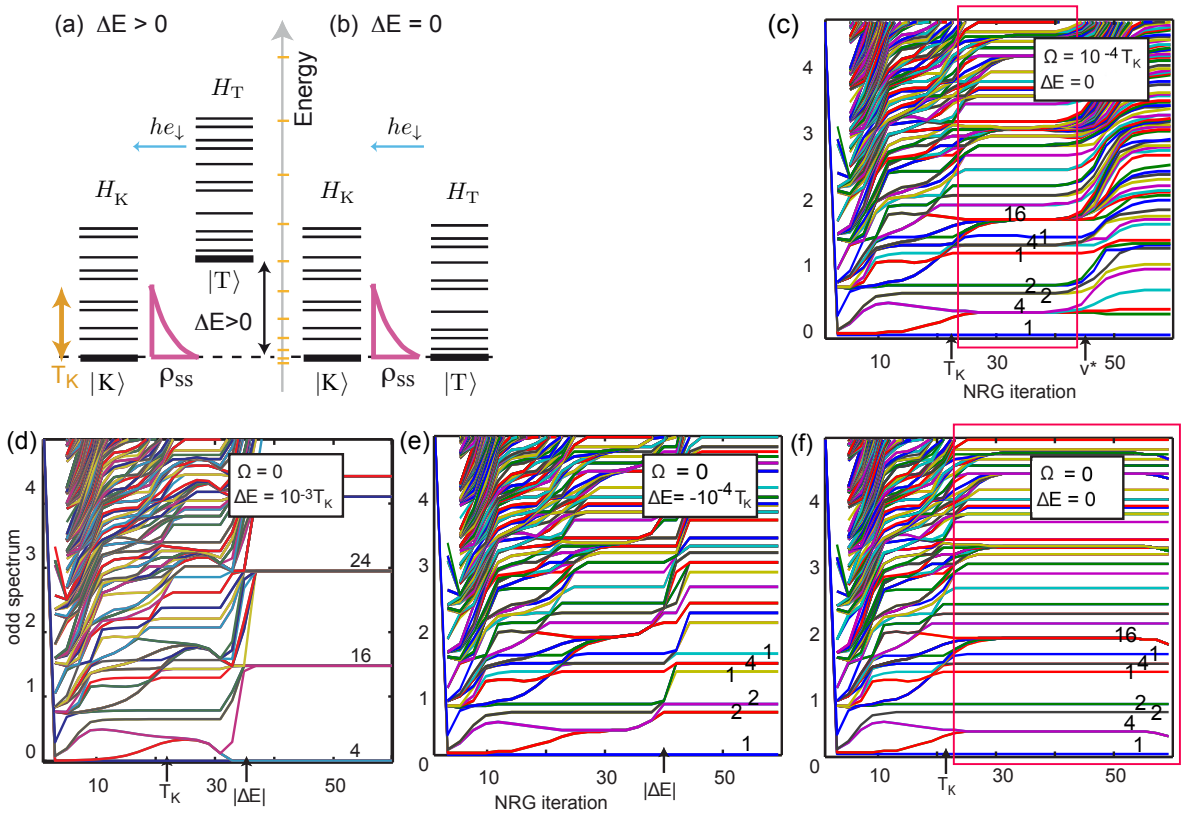

Figure S2: Effect of ΔE for one NRG diagonalization in the $\Omega = 0$ case: (a) $\Delta E > 0$ features a good resolution for the highly-correlated low-energy states above $|\mathrm{K}\rangle$, but not for the trionic states above $|\mathrm{T}\rangle$ and there is only a very small steady state hole population. (b) For $\Delta E = 0$, a good resolution for both families of states is achieved along with approximately equal steady state population in both ladders. (c) to (f): Flow diagrams for various parameter combinations ΔE and Ω, with the red box showing the intermediate fixed point $H|_{\Omega=0}$. The NRG parameters are: Discretization $\Lambda = 2.7$, number of kept states $N_{\mathrm{keep}} = 1800$ and chain length $N_{\mathrm{max}} = 60$. The model parameters are the same as in Fig. 2 in the main text and the numbers attached to the final fixed point levels denote the degeneracies of the respective eigenenergies.

To find the right laser energy to compensate the ground state energy difference and ensure $\Delta E = 0$, NRG flow diagrams are employed: Both Hamiltonians H_{T} and H_{K} have distinct and well understood low energy fixed points: The H_{K} fixed point [obtained by setting $\Delta E > 0$ and $\Omega = 0$, see Fig. S2 (d)] describes the primary Kondo singlet state and its excitations. The degeneracies for odd Wilson site indices n ('odd spectrum') are 4, 16,... . The H_{T} fixed point, describing the trion state and its excitations [$\Delta E < 0$ and $\Omega = 0$, see Fig. S2 (e)] features the degeneracies 1, 2, 2, 1, 4, 1,... . Consequently, since we still consider the uncoupled $\Omega = 0$ case, the H flow diagram for $\Delta E = 0$ [Fig. S2 (f)] consists of a combination of the flow diagrams of the two decoupled Hamiltonians H_{T} and H_{K}. This can be seen in detail by comparing state degeneracies (1, 4, 2, 2, 1, 4, 1, 16,...) which are a combination of the aforementioned degeneracies of H_{K} and H_{T}. We used this fact as a technical trick guiding us how δ_{L} should be fine-tuned to reach $\Delta E = 0$.

We now turn to the case where the trion and photon subspaces are coupled by stimulated absorption

and emission events for $\Omega > 0$. The parameter ΔE is still defined with respect to the $\Omega = 0$ case. Due to the discretization issues mentioned above, results for $|\Delta E| \gg \Omega$ should be regarded with care. We diagonalize the full Rabi-Kondo model, Eq. (S3). The flow diagram for $\Omega = 10^{-4} T_{\mathrm{K}}$ and $\Delta E = 0$ is shown in Fig. S2(c). We observe the emergence of a new fixed point below an energy scale

$$\nu^* \simeq \max\left(|\Delta E|, \Omega^*\right) \tag{S5}$$

which generalizes Ω^* from Eq. (5) for finite ΔE.

Between the scales T_{K} and ν^*, the fixed point spectrum for $\Omega > 0$ in Fig. S2 (c) has the same structure as the fixed point found for $\Omega = 0$ in Fig. S2 (f), as can be seen by comparison of the red boxes. Hence, the intermediate fixed point for $\Omega > 0$ in Fig. S2 (c) can be understood as a combination of H_{K} and H_{T}. This further implies that the QD-perturbation Ω, though local, only affects the system far away from the QD.

Eq. (S5) can be understood by noting that for finite $\Delta E^{(\prime)}$ the RG flow, Eq. (4), is augmented by a similar equation for $\Delta E'$ which, like the displaced charges, scales with $\Delta E'/D'$ and Ω'/D' in second order. Since $\Delta E'/D'$ and Ω'/D' are small initially compared to unity, $\Delta E'$ and U'_σ do not flow appreciably under RG. Consequently, in the RG flow, the normalized TLS parameters Ω'/D' and $\Delta E'/D'$ increase. As soon as the larger one reaches unity, the scaling equations lose validity. For $|\Delta E'| \ll \Omega^*$, the renormalized Rabi frequency Ω' will increase to the renormalized bandwidth D' before D' reaches $\Delta E'$ and we enter the strong-Ω fixed point below Ω^*, as discussed in the main text. If however $|\Delta E'| \gg \Omega^*$, the TLS energy splitting $\Delta E'$ determines the scale of the uncoupled fixed point, as expressed in Eq. (S5), for the unprimed parameters of the original model H.

The effect of Eq. (S5) on the broad peak position $|\nu_{\max}|$ of the emission spectrum is shown in Fig. S3(a). Analogously, the expression for the weight of the δ-peak is also modified with a cutoff at $|\Delta E| = \Omega^*$ (Fig. S3(b)). For $|\Delta E| \gg \Omega^*$ the ground state contains either the trion or the Kondo state, so that $\delta_{\mathrm{weight}} = |\langle h_{\Uparrow} e_{\downarrow}\rangle|^2$ vanishes due to AO between ground and post-quench state.

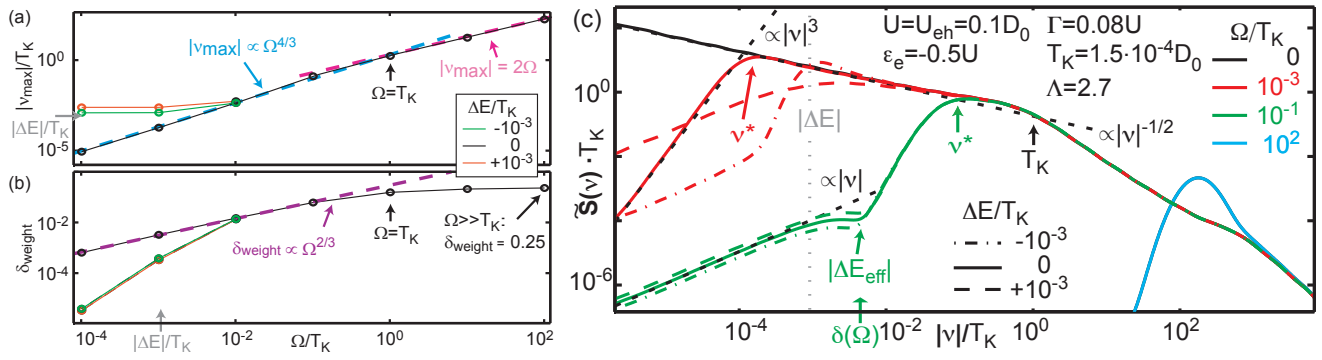

Figure S3: NRG results for the Rabi-Kondo model, Eq. (1), for finite ΔE: The position of broad peak $|\nu_{\max}|$ in (a) and the weight of $\delta-$peak in (b) both deviate from the $\Delta E = 0$ case at $\Omega^* \simeq \Delta E$ where the nature of the low energy fixed point changes according to Eq. (S5). (c) Log-log plot of the normalized broad emission peak ($\tilde{S}(\nu < 0)$, for details on the normalization see below) for various parameters Ω and ΔE. Thick solid lines denote spectra with $\Delta E = 0$, dashed and dash-dotted lines represent $\Delta E = \pm 10^{-3} T_{\mathrm{K}}$, respectively. The straight dashed lines represent power-law functions.

Quantum Quenches and Beyond: Anderson Orthogonality, Hopfield Rule and their application for $S(\nu)$

In this section, we provide some background information on the concept of Anderson Orthogonality (AO), the Hopfield Rule and their application in the discussion of the emission spectrum $S(\nu)$. The basic idea is that for $\Omega = 0$ spontaneous emission can be thought of as a transition corresponding to a quantum quench, showing AO, while for $\Omega \neq 0$, the signatures of AO are cut off at sufficiently low frequencies.

Anderson Orthogonality (AO) and Hopfield Rule (see also Ref. [6] for an extensive discussion): Whenever a quantum quench changes the local scattering potential for a FB, the overlap between the initial and final FB ground states, $|G_\mathrm{i}\rangle$ and $|G_\mathrm{f}\rangle$, vanishes with increasing electron number N as $|\langle G_\mathrm{i}|G_\mathrm{f}\rangle| \propto N^{-\frac{1}{2}\Delta_\mathrm{AO}^2}$ where Δ_AO is called the AO exponent. In the thermodynamic limit $N \to \infty$, the initial and final ground states are thus orthogonal for $\Delta_\mathrm{AO} \neq 0$. There are two important remarks: (i) Anderson [7] showed that the exponent Δ_AO equals the displaced electronic charge (in units of e) in the quench, i.e.

$$\Delta_\mathrm{AO} = \langle G_\mathrm{f}|n_\mathrm{tot}|G_\mathrm{f}\rangle - \langle G_\mathrm{i}|n_\mathrm{tot}|G_\mathrm{i}\rangle\,, \tag{S6}$$

where n_tot counts the (spinless) electrons in a large volume V_large including the scattering site (QD). For spinful fermions, if the spin-channels are decoupled such that the FB ground states factorize, the correspondence is generalized to

$$\Delta_\mathrm{AO}^2 = \Delta_{\mathrm{AO},\downarrow}^2 + \Delta_{\mathrm{AO},\uparrow}^2. \tag{S7}$$

Note that by Friedel's sum rule, the displaced charge is connected to the scattering phase shift δ_σ for electrons with spin $\sigma = \pm$ by $\Delta_{\mathrm{AO},\sigma} = \delta_\sigma/\pi$. (ii) AO has important consequences for the low frequency behavior of generic quench spectral functions $\mathcal{A}$ similar to $S(\nu)$ in Eq. (2). AO causes the spectral function to behave as $\mathcal{A}(\nu) \propto \nu^{-1+\Delta_\mathrm{AO}^2}$, where ν is measured with respect to a threshold frequency.

Application of AO to emission spectrum $S(\nu)$: We start our discussion with the quench Hamiltonian $H|_{\Omega=0} = H_\mathrm{QD,L} + H_\mathrm{QD-FB} + H_\mathrm{FB} = H_\mathrm{K} + H_\mathrm{T}$ which we represent schematically in Fig. S4(a). The dashed line between the QD (circle) and the FB (box, in Wilson chain approximation) represents a tunnel coupling, the horizontal axis denotes decreasing energy or increasing length scales as in a NRG flow diagram (see above). If we assume $\Delta E = 0$, the degenerate ground state $|G\rangle\,|_{\Omega=0}$ is a superposition of the trionic state $|\mathrm{T}\rangle$, ground state of H_T shown in (b), and the Kondo singlet state $|\mathrm{K}\rangle = (|\uparrow\rangle\,|\mathrm{FB}_\downarrow\rangle - |\downarrow\rangle\,|\mathrm{FB}_\uparrow\rangle)/\sqrt{2}$, ground state of H_K, depicted in (c). While $|\mathrm{K}\rangle$ features strong correlations between QD and FB, the trion state can be well approximated as a simple QD-FB product state $|\mathrm{T}\rangle = |\uparrow\downarrow\Uparrow\rangle\,|\mathrm{FB}_0\rangle$ where $|\mathrm{FB}_0\rangle$ is the unperturbed Fermi sea, i.e. all Wilson sites are half occupied. Let us take the state $|\mathrm{K}\rangle$ as reference, where the QD valence levels are filled (no holes present) and its conduction levels harbor half an electron of each spin. The region where the FB parts of the $|\mathrm{K}\rangle$ state, $|\mathrm{FB}_\sigma\rangle$, support an additional spin σ (the screening cloud) is encircled by a yellow ellipse. Relative to $|\mathrm{K}\rangle$, the state $|\mathrm{T}\rangle$ features displaced charges $\Delta_{\mathrm{T},\sigma} = \sigma/2$, respectively (the $\Uparrow$-hole counts like a missing $\downarrow$-electron). Before discussing emission, let us consider an absorption event. Acting on $|G\rangle\,|_{\Omega=0}$ with the operator $e_\downarrow^\dagger h_\Uparrow^\dagger$, we first project on the component $|\mathrm{K}\rangle$ and then create a hole and a spin down electron in the conduction level. The resulting state can "lower its energy" [8] by adjusting its spin configuration to the $|\mathrm{T}\rangle$ state (b).

A priori, it is not obvious how an absorption process described by the operator $e_\downarrow^\dagger h_\Uparrow^\dagger$ for Hamiltonian

H can be treated in the framework of AO. First, we recall a non-trivial feature of the Anderson impurity model underlying $H_{\rm K}$, namely that the low-energy fixed point below $T_{\rm K}$ can be described by potential scattering off the complicated Kondo screening cloud structure [5]. This observation implies that AO plays a role only for $|\nu| < T_{\rm K}$, as documented by an $-1/2$ power-law tail [5] which is explained as follows: Comparing the final state $|{\rm T}\rangle$, to the initial state $|{\rm K}\rangle$, the displaced charges (Eq. (S6)) read $\Delta_\sigma \equiv \Delta_{{\rm T},\sigma} - \Delta_{{\rm K},\sigma} = \sigma/2$. Consequently, for the quench connecting these two ground states in the long time limit, we find from Eq. (S7)

$$\Delta_{\rm AO}^2 = \Delta_{{\rm AO},\downarrow}^2 + \Delta_{{\rm AO},\uparrow}^2 = (\Delta_{{\rm T},\uparrow} - \Delta_{{\rm K},\uparrow})^2 + (\Delta_{{\rm T},\downarrow} - \Delta_{{\rm K},\downarrow})^2 = 0.5. \tag{S8}$$

Since only the magnitude of the displaced charges, $(\Delta_{{\rm T},\sigma} - \Delta_{{\rm K},\sigma})^2$, enters this equation, $\Delta_{\rm AO}^2$ and the $-1/2$ power-law tail is the same for the emission process.

The second issue is the presence of the coherent laser drive, $H_{\rm QD-L} \propto \Omega$ in H leading to stimulated absorption and emission processes. Thus spontaneous emission or absorption does *not* introduce a quantum quench, since the subspaces $P_{\rm T}$ and $P_{\rm K}$ are not dynamically decoupled [9]. However, if Ω is small, we can expect that the post-emission dynamics is not affected by the existence of Ω up to some time $\tau = 1/\Omega^*$ (i.e. $e^{i\tau H}(h_{\Uparrow}e_{\downarrow})^\dagger e^{-i\tau H} \simeq e^{i\tau H|_{\Omega=0}}(h_{\Uparrow}e_{\downarrow})^\dagger e^{-i\tau H|_{\Omega=0}}$ in Eq. (S1) for $\tau < 1/\Omega^*$) and that the spectral function therefore shows AO behavior as in a proper quench situation for $|\nu| > \Omega^*$. The relation between Ω^*, Ω and the displaced charges can be found by a renormalization group analysis as sketched in the main text.

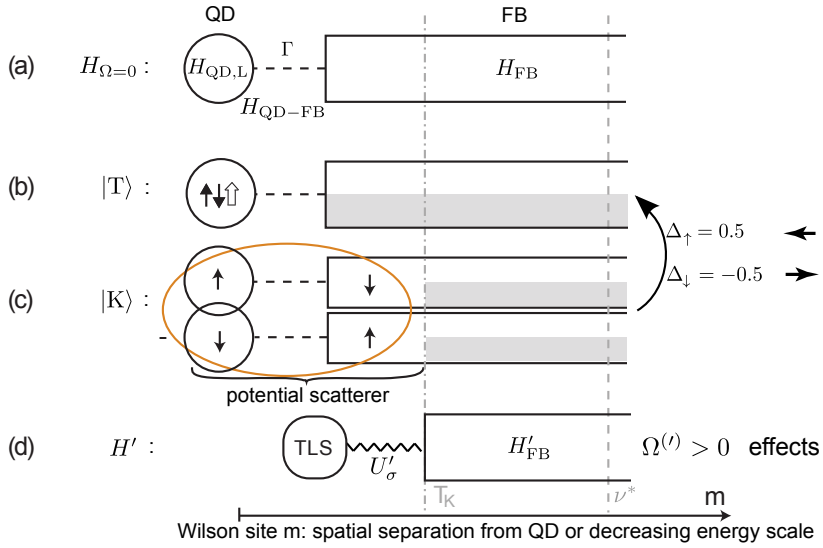

Figure S4: Cartoon of some Hamiltonians and states mentioned in the main text. (a) The quench Hamiltonian $H|_{\Omega=0}$ is of quantum impurity type, featuring a local QD and laser part tunnel coupled to the extended FB. The trionic state (b) can lower its energy after a spontaneous emission process mediated by $h_{\Uparrow}e_{\downarrow}$ by the formation of correlations (c) between QD and surplus FB spins where the latter are contained in a region of extent $1/T_{\rm K}$ around the QD (yellow ellipse). The Kondo singlet and trion configuration both act as potential scatterers for the surrounding FB electrons. The effective Hamiltonian H', which explicitly contains a potential scattering term $\propto U'_\sigma$ in the trion sector, reproduces the respective scattering phase shifts of (b) and (c). In any case, effects due to $\Omega > 0$ are relevant above length scales $1/\nu^*$.

Effective model H'

Considering the NRG energy flow diagrams of the Rabi-Kondo model H in Fig. S2 we noticed that the intermediate fixed point spectrum above ν^* is composed simply of a combination of the spectra of H_{K} and H_{T}. This shows that in this intermediate energy range, the spectrum of the full Hamiltonian space can be decomposed into a direct sum of two subspectra, one describing the primary Kondo singlet state and its excitations, the other the trion and its excitations. These get coupled only at energy scales below ν^*. This fact is the main motivation for constructing the effective Hamiltonian H'.

Before comparing H and H' NRG energy flow diagrams, we augment the heuristic derivation of the effective model H' given in the main text in Eq. (3) by an intuitive graphical explanation in Fig. S4. The effective model H' denoted schematically in Fig. S4(d) is designed to describe the effect of the transition between $|\mathrm{T}\rangle$ and $|\mathrm{K}\rangle$ [from (b) to (c)] on FB electrons beyond a separation $1/T_{\mathrm{K}}$ from the QD. The two-level-system (TLS), representing the QD plus the FB up to distance $1/T_{\mathrm{K}}$, controls the scattering potential U'_σ [wavy line in (d)] for the surrounding FB electrons. If the TLS changes its state, so does the scattering potential – not only after a time scale $1/T_{\mathrm{K}}$ but (within the approximation of replacing H by H') instantaneously like in a X-ray absorption process. For $\Omega' = 0$, σ'_z is conserved and the displaced electronic charge in a transition from $|\mathrm{K}\rangle_r$ to $|\mathrm{T}\rangle_r$ (TLS raising operators) is $\Delta'_\sigma = -1/\pi \cdot \arctan\left(\pi\rho' U'_\sigma\right)$ (in units of e, e.g. [6]). To reproduce the displaced charge $\Delta_\sigma = \sigma/2$ as found above, we require $\rho' U'_\sigma$ being equal to $-\sigma$ times a numerical value large compared to unity (we take $\rho' U'_\sigma = -50 \times \sigma$).

Now we can also consider the coherent QD-laser coupling. It is not a priori clear that H' as given in Eq. (3), and the reasoning laid out above, would still be applicable for $\Omega^{(\prime)} > 0$. However, our NRG calculations show (in accordance with a renormalization analysis and the discussion below Eq. (S5)) that the $H|_{\Omega>0}$ flow diagram does not differ from the $\Omega = 0$ case for energies higher than ν^* (compare Figs. S2(c) and (f)), implying that it is indeed valid to consider the development of potential scattering and the effects of Ω *separately* as long as $\nu^* \ll T_{\mathrm{K}}$.

NRG energy flow comparison for H and H': One of the implicit assumptions in replacing H by the effective Hamiltonian H' with the scattering phase shifts as given above is that $n_{\mathrm{e}\uparrow} + n_{\mathrm{e}\downarrow} - n_{\mathrm{h}}$ exactly equals one. With the physical parameters as in Fig. 2 in the main text, this is only approximately true due to $U_{\mathrm{eh}} < \infty$. Although this small deviation has no observable consequences in the emission spectrum, turning to NRG energy flow diagrams resolving minute details of eigenstates and -energies, this issue will matter. Therefore, as an intermediate step for a flow diagram bases comparison of H and H', in Fig. S5 (a)-(c) we show the (odd) flow diagrams for $H|_{U_{\mathrm{eh}}=100D_0}$ where, as compared to the original H spectra in Fig. S2, certain degeneracies in the trionic sector are restored. These flow diagrams then indeed agree with those for the effective model H' [panels (d)-(f)].

Discussion of emission spectra for $H^{(\prime)}$ in the case $\Delta E^{(\prime)} \neq 0$

In Fig. S3(c), the Rabi-Kondo model emission spectrum, shown in Fig. 2(b,c) of the main text, is repeated for finite ΔE. Since the total spectral weight is given by $\langle n_{\mathrm{h}} n_{\mathrm{e}\downarrow}\rangle \simeq O\left(\langle n_{\mathrm{h}}\rangle\right)$, it is strongly dependent on ΔE. To enable mutual comparison between results for different values of ΔE we normalize all NRG spectra in this Supplemental Material as $\tilde{S}(\nu) \equiv S(\nu) / \langle n_{\mathrm{h}}\rangle$. Fig. S6(a) schematically summarizes the

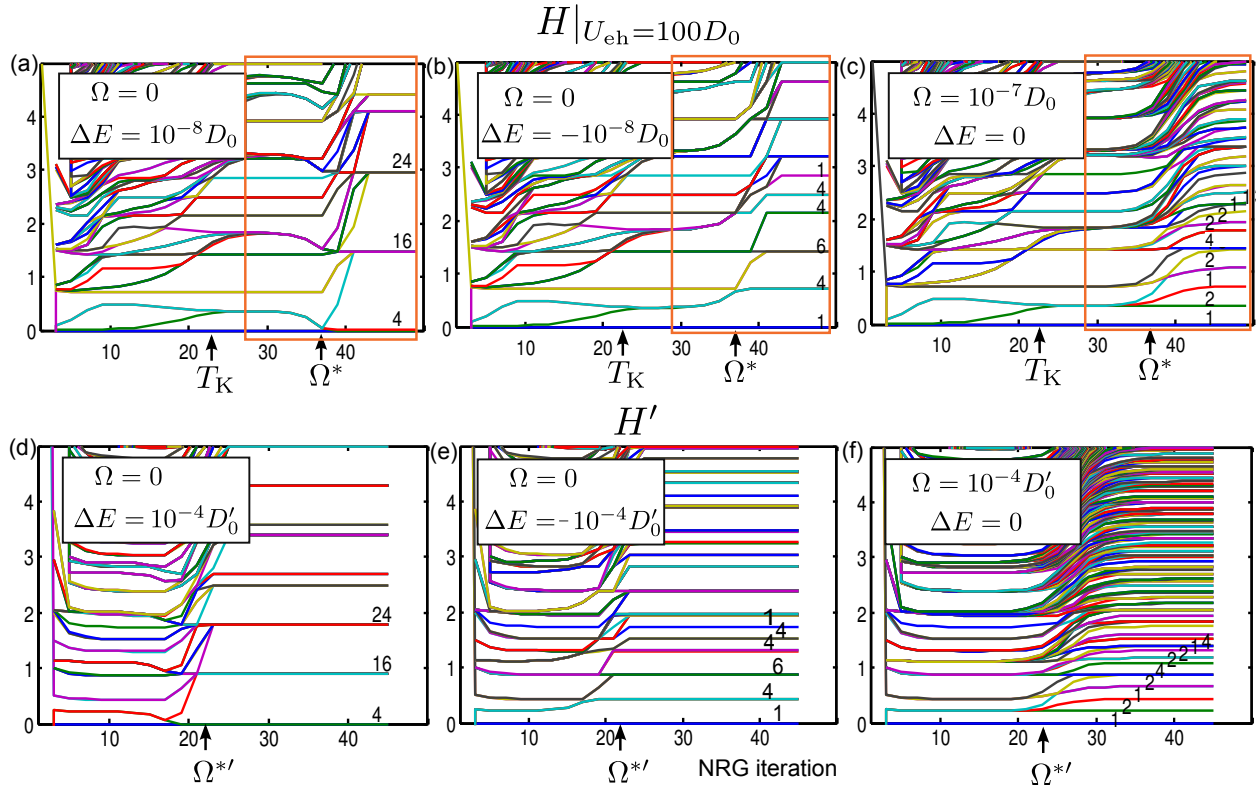

Figure S5: Comparison of NRG energy flow diagrams for $H|_{U_{\rm eh}=100D_0}$ [panels (a)-(c)] and H' [panels (d)-(f)] for $\Delta E^{(\prime)} \lessgtr 0$ and $\Omega^{(\prime)} > 0$. With the QD/TLS defined as Wilson site zero, the $H|_{U_{\rm eh}=100D_0}$ flow diagrams show odd NRG iterations and the H' diagrams even iterations such that an odd number of Wilson sites has been integrated out in going from H to H'. The H' flow diagrams mimic those of portions [boxed] of the $H|_{U_{\rm eh}=100D_0}$ flow diagrams that show the crossover from the intermediate to the strong-coupling fixed point.

generic features of the line shape. Coming from large detunings $|\nu|$, the characteristic power-law tails with exponents -2 (in the free orbital (FO) regime), -1 (in the local moment (LM) regime) and $-1/2$ (in the strong coupling (SC) regime), found and discussed by Türeci *et al.* in Ref. [5], are present also for $\nu^* < T_{\rm K}$. Curly brackets indicate the range of validity of several Hamiltonians mentioned in the main text. While treating Ω perturbatively using the quench Hamiltonian $H|_{\Omega=0}$ is a valid approximation for $|\nu| > \nu^*$, the effective Hamiltonian in Eq. (3) provides the appropriate approximate description for $|\nu| < T_{\rm K}$ and can explain the emergence of the low energy fixed point below ν^*. The RF spectrum for the effective Hamiltonian H', calculated using Eq. (2) but with H' and σ'_- taking the place of H and $h_\Uparrow e_\downarrow$, respectively, is shown in Fig. S7. It indeed correctly reproduces all features of the H spectrum for $|\nu| < T_{\rm K}$, which we now discuss.

The fixed point at energy ν^* causes a cut-off of the emission line shape; the nature of the line shape below the cut-off energy depends on ΔE and Ω. Fig. S6(b) explains this regime $0 < |\nu| < \nu^*$ in detail, where we find a combination of $+3$ and $+1$ power-law tails as indicated schematically. We consider the two cases $\Omega^* \lessgtr |\Delta E|$ separately.

(i) For $\Omega^* > |\Delta E|$, the transition between the $+3/+1$ power-law tails occurs at a scale

$$\Delta E_{\text{eff}} = \Delta E + \delta(\Omega) > \Delta E, \tag{S9}$$

where $\delta(\Omega)$ denotes an Ω-dependent effective detuning with $0 < \delta(\Omega) \ll \Omega$ that captures the small driving dependence which is attributed to second-order effects in the RG equations for $\Delta E'$ discussed above. The $+3/+1$ crossover is either sharp for $\Delta E_{\text{eff}} > 0$ or gradual in the case $\Delta E_{\text{eff}} < 0$. The analysis for the $+1$ exponent parallels the discussion for the $+3$ exponent in terms of the secondary Kondo model H'_{K} given in the main text: The presence of an effective magnetic field ($\Delta E_z \neq 0$) in Eq. (6), corresponding to a finite $\Delta E^{(\prime)}$ in models H and H', causes the density of the z-component of the spin in H'_{K} to acquire a nonzero average. Hence, the correlation function $S'_z s'_z(0)$ will have components containing the correlator of just two Fermi operators with their conjugates, which decays as t^{-2}, leading to a $\sim |\nu|^{+1}$ behavior of the spectral function.

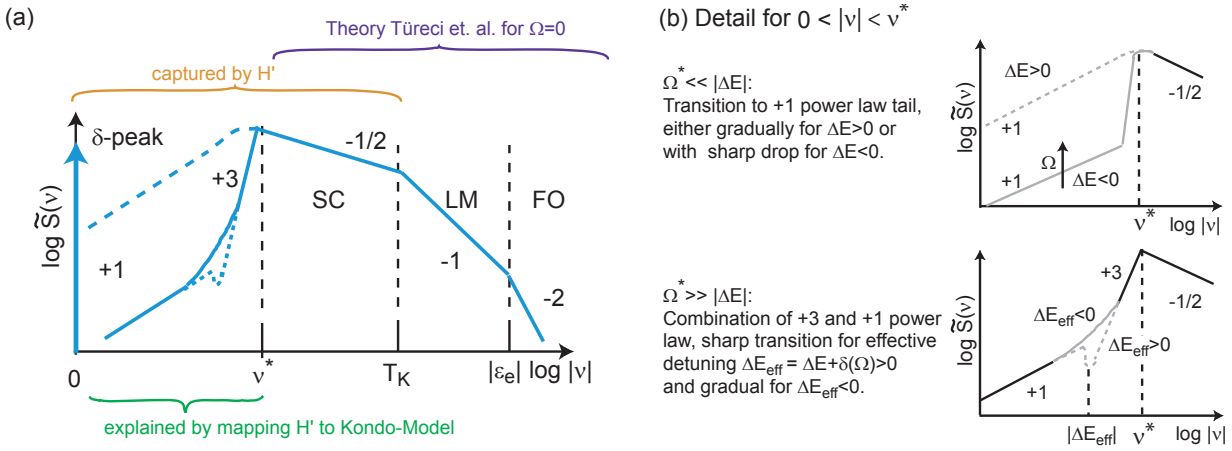

Figure S6: Phenomenological discussion of $\tilde{S}(\nu)$, revealing characteristic power-law tails. The same discussion applies to $\tilde{S}'(\nu)$ (for the effective Hamiltonian H') for $|\nu| < T_{\text{K}}$.

The effect described in Eq. (S9) can be clearly seen in the H spectrum for $\Delta E = 0$ (Fig. S3(c), $\Omega = 10^{-1} T_{\text{K}}$, green solid line) which shows a transition to a $+1$ tail at $\Delta E_{\text{eff}} = \Delta E + \delta(\Omega) = \delta(\Omega)$. Further, the $\Omega = 10^{-1} T_{\text{K}}$ spectra for $\Delta E = \pm 10^{-3} T_{\text{K}}$ (green dashed and dash-dotted lines) do not differ significantly since we have $\delta(\Omega) \gg \Delta E$ and thus, according to Eq. (S9), ΔE_{eff} is virtually equal in both cases.

(ii) Turning to $\Omega^* < |\Delta E|$, (dash and dashed-dotted red lines in Fig. S3(c)) the $+3$ tail is absent; in the case $\Delta E > 0$ a smooth transition to the $+1$ tail occurs while for $\Delta E < 0$ this transition is realized in a steep drop beyond NRG's smoothing resolution limit. This steep drop can be understood in the limiting case $\Omega \to 0$ as a horizontally displaced $\Omega = \Delta E = 0$ curve which has a threshold at $|\nu| = -\Delta E$.

Implications for an experimental study and outlook

The NRG results shed light on the results of the competition between Kondo physics and the laser coupling. As expected, the ratio of T_{K} and Ω determines the predominant form of the emission line shape, an asymmetric power-law-divergent peak in the Kondo-dominated regime $\Omega \ll T_{\text{K}}$, and a double

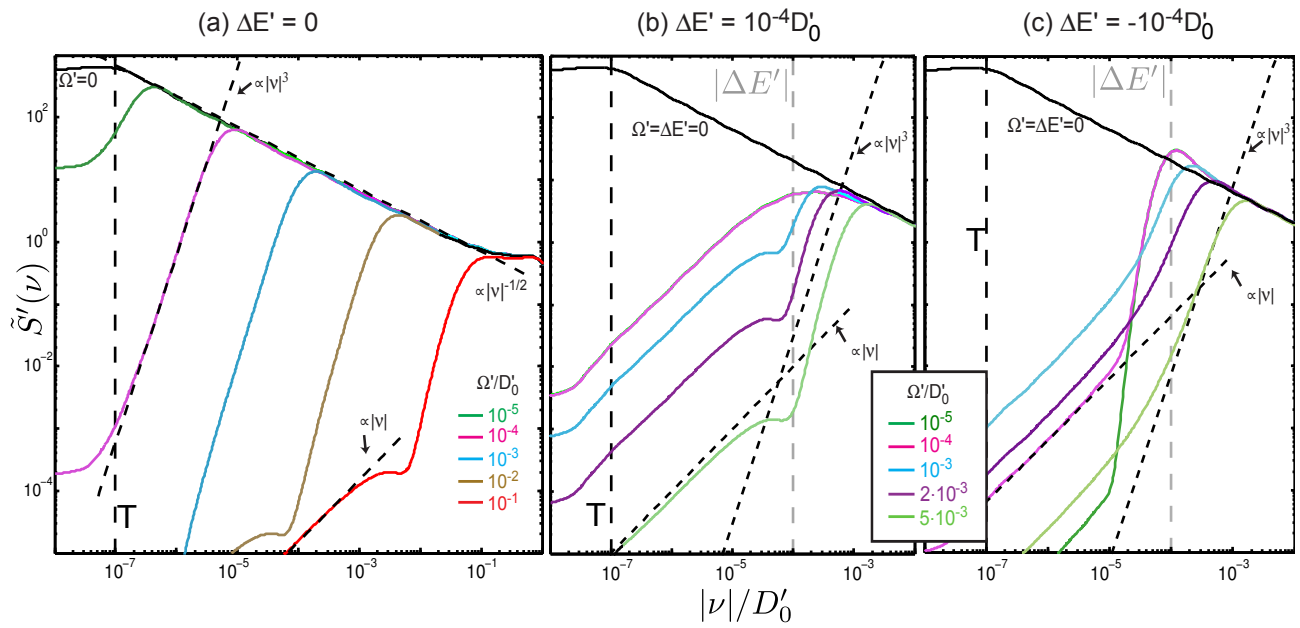

Figure S7: $\tilde{S}'(\nu<0)$ for H' (without $\delta-$peak). (a) $\Delta E'=0$, (b) $\Delta E'>0$ and (c) $\Delta E'<0$. For reference, the $\Omega'=\Delta E'=0$ spectrum is repeated in all plots (solid black line).

peak structure in the limit $\Omega \gg T_{\rm K}$. However, the role of the seemingly weaker effect is interesting: A dominant driving laser leaves no trace of Kondo physics while dominant Kondo physics renormalizes Ω to a smaller value but preserves its characteristic non-trivial double peak feature in the spectrum. This explains our focus on the regime $\Omega < T_{\rm K}$, which is highly attractive for further experimental study. We remark that the main results should be also valid in a two laser setup (creating dressed states with one laser, probing absorption with another), which might be experimentally more feasible than standard resonance fluorescence.

For a strongly coupled device and temperatures $T \ll T_{\rm K}$, Kondo signatures in the absorption line shape of a weak laser have already been detected in experiment [10]. An order of magnitude separation between T (which flattens out all spectra for $|\nu| \lesssim T$) and $T_{\rm K}$ as well as a spontaneous emission rate below T has been achieved. For obtaining the predicted double peak structure in the resonance fluorescence experiment with $\Omega < T_{\rm K}$, the crucial condition $T \ll \nu^* \ll T_{\rm K}$ has to be fulfilled. We expect that a non-zero spontaneous emission rate will lead to partial broadening of the δ-peak at zero detuning, separating into an elastic and inelastic component. For the proper inclusion of spontaneous emission in the theoretical treatment, we propose an extension of the current study using the framework of Lindblad-NRG, currently under development [11].

The total area of the peak at the laser frequency and the peak-to-peak separation to the red emission peak are predicted to scale with Ω to the power 2/3 and 4/3, respectively. This is valid if ΔE (controlled by the laser detuning) is smaller than the renormalized Rabi frequency Ω^*. Compared to the measurement of power-law tails as signatures of Kondo physics, which require experimental data with sufficiently low noise level, peak areas and peak-to-peak separations can be measured with relative ease. Further, the scaling collapse of the broad emission peak with respect to ν^*, which is theoretically valid only for $S(\nu)$

with $|\Delta E_{\rm eff}| < |\nu| < T_{\rm K}$, should be a robust experimental feature since the regions where scaling fails (i.e. $|\nu| > T_{\rm K}$, $|\nu| < |\Delta E_{\rm eff}|$) are expected to support only a small spectral signal, effectively well below the noise level.

It is interesting to compare the effect of a laser drive Ω with the consequences of a nonzero magnetic field B (which we have set to zero throughout this work). While a circularly polarized laser coupling in a QD removes the degeneracy of the spin up and down state just like a magnetic field B does, their signatures in the emission spectrum in presence of Kondo physics are strikingly different. While a magnetic field $|B| < T_{\rm K}$ results in a smooth modification of the $B = \Omega = 0$ fixed point (and consequently changes the $-1/2$ power-law exponent in the RF line shape [5, 10]) a Rabi frequency $\Omega < T_{\rm K}$ induces a *new* low energy fixed point while keeping the power-law exponent at $-1/2$. For nonzero B *and* Ω (both $< T_{\rm K}$) we conclude that a modification of the Ω-scaling dimension η_x (in the original Rabi-Kondo model) due to B would modify the 4/3 and 2/3 exponents for the Ω^* and $\delta_{\rm weight}$-scaling with Ω. Thus, application of a magnetic field could enhance the visibility of scaling effects on the emission spectrum in experiment.

References

[1] B. Sbierski, A. Imamoglu. (to be published).

[2] H. Breuer, F. Petruccione, *The Theory of Open Quantum Systems* (Oxford, 2002).

[3] C. Cohen-Tannoudji, J. Dupont-Roc, G. Grynberg, *Atom-Photon Interactions* (Wiley, 1992).

[4] R. Bulla, T. A. Costi, T. Pruschke, *Rev. Mod. Phys.* **80**, 395 (2008).

[5] H. E. Türeci, *et al.*, *Phys. Rev. Lett.* **106**, 107402 (2011).

[6] W. Münder, A. Weichselbaum, M. Goldstein, Y. Gefen, J. von Delft, *Phys. Rev. B* **85**, 235104 (2012).

[7] P. W. Anderson, *Phys. Rev. Lett.* **18**, 1049 (1967).

[8] Of course, unitary evolution cannot change a state's energy and evolve the post quench state to the Kondo singlet state. More precisely, consider the overlap between post-emission state and its time-evolved version in Eq. (S1): Expanding in energy eigenstates, for times larger than $1/T_K$ the overlap has contributions only from strongly correlated eigenstates below energy T_K.

[9] However, spontaneous emission can be interpreted as a quench between two adjacent excitation manifolds in the dressed state picture of resonance fluorescence.

[10] C. Latta, *et al.*, *Nature* **474**, 627 (2011).

[11] I. Weymann, A. Weichselbaum, J. von Delft, *(to be published)* .